The Cryosphere
Discussions
Open Access
EGU

1 # Snow Avalanche Frequency Estimation (SAFE): 32 years of remote hazard

2 # monitoring in Afghanistan

3 Arnaud Caiserman[1*], Roy C. Sidle[1], Deo Raj Gurung[2]

4 [1] Mountain Societies Research Institute – University of Central Asia, Khorog, 736000, Tajikistan

5 A. Caiserman ORCID: https://orcid.org/0000-0003-4580-6633 ; corresponding author: arnaud.caiserman@ucentralasia.org

6 Roy C. Sidle ORCID: https://orcid.org/0000-0002-5004-4154

7 [2] Aga Khan Agency of Habitat, Dushanbe, 734013, Tajikistan

8 Deo Raj Gurung ORCID:

9 *Correspondence to*: Arnaud Caiserman (arnaud.caiserman@ucentralasia.org)

10 **Abstract.** Snow avalanches are the predominant hazards in winter in high elevation mountains. They cause damage

11 to both humans and assets but cannot be accurately predicted. Until now, only local maps to estimate snow

12 avalanche risk have been produced. Here we show how remote sensing can accurately inventory large avalanches

13 every year at a basin scale using a 32-yr snow index derived from Landsat satellite archives. This Snow Avalanche

14 Frequency Estimation (SAFE) built in an open-access Google Engine script maps snow hazard frequency and

15 targets vulnerable areas in remote regions of Afghanistan, one of the most data-limited areas worldwide. SAFE

16 correctly detected of the actual avalanches identified on Google Earth and in the field (Probability of Detection

17 0.77 and Positive Predictive Value 0.96). A total of 810,000 large avalanches occurred since 1990 within an area

18 of 28,500 km^2 with a mean frequency of 0.88 avalanches/km^{2}yr^{-1}, damaging villages and blocking roads and

19 streams. Snow avalanche frequency did not significantly change with time, but a northeast shift of these hazards

20 was evident. SAFE is the first robust model that can be used worldwide and is capable of filling data voids on

21 snow avalanche impacts in inaccessible regions.

22

23 ## 1. Introduction

24 Snow avalanches are among the fastest, up to 61 m/s^{-1}, and therefore most dangerous natural hazards in mountain

25 areas (Louge et al., 2012). Casualties associated with avalanches are numerous; in 2021 alone, 37 fatalities occurred

26 in the US (Colorado Avalanche Information Center, 2021) and 127 in Europe (European Avalanches Warning

27 Services, 2021), but avalanche monitoring is not consistent across the globe. Most remote mountain regions and

28 communities are not systematically monitored for avalanche occurrence. Avalanche surveys amongst remote

29 villages are sparse because regions are uninhabited; however, avalanches can block connecting roads every year

30 since avalanche volumes range from hundreds to several tens of thousand cubic meters (Gubler, 1987). Where

31 weather stations exist, avalanches can be predicted based on snow depth and other weather parameters (Greene et

32 al., 2016). However, the global weather monitoring of mountainous areas is scattered and very sparse in developing

33 nations.

34   To support these science and government priorities in remote mountain regions, it is necessary to introduce a user-
35   friendly, open-access method that maps snow avalanches on an annual basis across wide areas where internet
36   connection and monitoring systems are not always available. As an example, half of the land surface of
37   Afghanistan is above 2000 m a.s.l. and 80% is mountainous (Asad Sarwar, 2002). Among Central Asian nations,
38   Afghanistan's population is most at risk of avalanche hazards; 22,477 inhabitants at risk compared to 5183 in
39   Tajikistan (Chabot and Kaba, 2016). Particularly, northeast Afghanistan (Badakhshan) is one of the most
40   vulnerable regions, especially from December through March (Mohanty et al., 2019). Several international
41   initiatives have been implemented in Afghanistan to forecast avalanches or assess their risks on local communities.
42   According to USAID, 30,600 buildings are at risk of avalanches in Badakhshan based on daily snow depth
43   measurements (USAID, 2021). The Aga Khan Agency for Habitat (AKAH) collects snow depth data and uses
44   models such as Alpine3D and SNOWPACK to forecast avalanche prone regions in Tajikistan, Afghanistan, and
45   Pakistan (Bair et al., 2020). Other products have been developed, such as avalanche susceptibility and exposure
46   maps (Kravtsova, 1990; World Bank, 2017). Another approach is to combine topographic maps and snow data via
47   the RAMMS:AVA models (GFDRR, 2018), but these are not open access. Finally, it is possible to count the
48   number of avalanches in each district as done by the United Nations in their map *Districts Affected by Avalanches*
49   (OCHA-United Nations, 2012), but this would be time consuming and may miss some events across large areas.
50   Detecting the avalanches is a challenge and requires temporal as well as spatial data, especially for large areas.
51   Remote sensing technology, both air and spaceborne, can cover large areas at different times of the year. Indeed,
52   the frequent collection of satellite images over the same area enables the detection of changes in snow cover as
53   well as other hazards, such as floods and landslides. Until recently, the use of remote sensing in avalanche detection
54   was sparse due to low resolution, and the automation of such processes was even more difficult because of the
55   lack of relevant algorithms that can compute big data (Eckerstorfer et al., 2016). Other remote sensing approaches
56   for avalanche detection have used radar, Lidar, and optical data. Radar satellites, such as Sentinel-1A and B, are
57   now commonly used for detecting mass movements by assessing backscatter signal changes between two time
58   periods (before and after movement) by a co-registration of the two images. Backscatter values provide
59   information on terrain roughness and any change indicates that a mass movement or a significant erosion event
60   occurred in a given area. This technology seems very promising for avalanche detection (Eckerstorfer et al., 2017;
61   Malnes et al., 2015; Martinez-Vazquez and Fortuny-Guasch, 2008; Schaffhauser et al., 2008; Tompkin and Leinss,
62   2021; Yang et al., 2020). However, the acquisition of frequent radar images is too recent to use this technique to
63   detect historical avalanches. Lidar is being used in the same regard with a higher level of precision. Lidar sensors
64   measure snow depth before and after events at submeter resolutions (Prokop, 2008; Deems et al., 2013; Prokop et
65   al., 2013; Hammond et al., 2018). However, this technology remains very expensive, and the spatial coverage is
66   limited. Therefore, Lidar data are not suitable for avalanche detection at a basin scale.

67   Optical data are the most available data in terms of spatial and temporal resolution as well as historical data

68   archives. Thus, we used optical data to detect avalanches on a long-term basis. Landsat-5, 7 and 8 products were

69   used as their resolution (30 m, 900 m²) is sufficient to detect small avalanches (Eckerstorfer et al., 2016). Most of

70   these data are available at a global scale. Optical sensors can detect areas covered or not covered by snow and this

71   approach has been used in multiple studies during the past decade. Manual approaches or indices have been used

72   in such studies. For example, Landsat-8 Panchromatic images (15 m) in combination with radar images were used

73   to detect avalanches in Norway (Eckerstorfer et al., 2014). Such combinations were also recently used in west

74   Greenland to map a large number of avalanches after an unprecedented snow event (Abermann et al., 2019). To

75   our knowledge, only one recent study automated the detection of avalanches using remote sensing products and

76   an open-access scripting approach (Smith et al., 2020). This study downloaded avalanches annually for a given

77   region of interest using available Landast-8 images and computed NDSI for each image. NDSI differentiated so

78   called 'supraglacial debris' from snow cover, for the date of interest. However, this approach only covers high

79   elevations areas while our study aims to detect avalanches proximate to local communities at lower elevations

80   (typically valleys). Manual and visual approaches, despite the time consuming process, can also be applied to

81   detect avalanches using high resolution images (e.g., SPOT-6), mid-resolution (e.g., Sentinel-2A and B images),

82   or even Google Earth images (Singh et al., 2020; Yariyan et al., 2020; Hafner et al., 2021). Terrain parameters like

83   slope gradient and curvature have also been added to the avalanche detection process using Digital Elevation

84   Models (DEM) combined with Landsat-8 images (Bühler et al., 2018; Singh et al., 2019). Integrated criteria are

85   therefore recommended to detect the avalanches. To our knowledge, no such studies using remote sensing have

86   been conducted in the world, especially not in Afghanistan.

87   The general objective of this study is to map annual avalanche occurrence over the past 32 years using Landsat

88   images archives in Badakhshan region, Afghanistan. Such long-term monitoring is a first attempt globally and

89   enables us to map the frequency of avalanches that impact valley communities. Thus, we used optical data to detect

90   avalanches on a long-term basis and built an open-access script in Google Engine interface: *Snow Avalanche*

91   *Frequency Estimation* (SAFE). Landsat-5, 7 and 8 products were used as their resolution (30 m, i.e., minimum

92   detectible size of 900 m²) is sufficient to detect larger avalanches (Abermann et al., 2019; Eckerstorfer et al., 2016,

93   2014; Hafner et al., 2021; Singh et al., 2019, 2020; Smith et al., 2020; Yariyan et al., 2020). Our objective is to

94   automatically map annual avalanche occurrence over the past 32 years using Landast-5, 7 and 8 image archives in

95   the Amu Panj basin of Afghanistan. Such long-term monitoring is a first attempt globally and enables us to map

96   the frequency of avalanches that impact remote mountain valley communities. These outputs are of keen interest

97   to decision makers who can use this automated process to map avalanche hazard in the future. The most vulnerable

98   areas, villages and roads, were mapped for improve future planning. In addition, this research enables the

99   monitoring of avalanche evolution over the past 32 years. Such analyses should strengthen local community

100   resilience to snow avalanches.
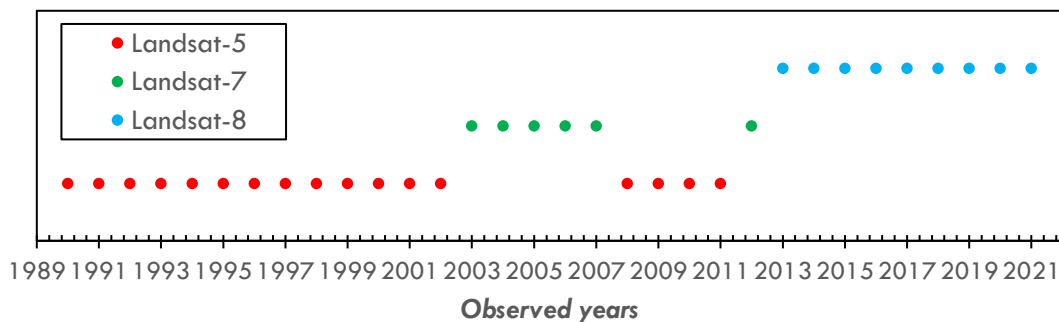
101

102   **2. Materials and methods**

103   **2.1 Study Area**

104   The study covers the most mountainous region of Afghanistan – Badakhshan in the Amu Panj basin located in the

105   northeast portion of the country. Average elevation is 2761 m and mean slope gradient is 21%. This region spans

106   from Bamyan Province to the Hindu Kush range, up through the Wakhan corridor in the far east of Afghanistan.

107   The summit is Nowshak Peak at an elevation of 7492 m a.s.l. The western part of Amu Panj basin is rather flat

108   and not prone to avalanches. Annual precipitation is 600 mm occurring mostly as snow between February and

109   May (Zhang et al., 2015). This terrain and precipitation characteristics lend Badakhshan very prone to avalanches.

110   The basin is large (28,580 km²), justifying automated avalanche detection to cover this area in a reasonable amount

111   of time using Google Engine. Despite the remoteness of this region, Badakhshan has a population of 950,953

112   inhabitants (Islamic Republic of Afghanistan Governmental Website, 2021) distributed in 4154 villages, mainly in

113   valleys. However, 35% of the villages in Badakhshan are located at elevations above 2000 m, increasing the

114   vulnerability of these communities to avalanches.

115

116   *2.2 Landsat Archives for Snowpack Analysis*

117   This analysis requires the integration of numerous data into a Google Engine Java script. Firstly, a mosaic of

118   different Landsat images is created every year in the Amu Panj basin. Depending on the year of interest, Landsat-

119   5   (https://developers.google.com/earth-engine/datasets/catalog/LANDSAT_LT05_C01_T1_SR)   Landsat-7

120   (https://developers.google.com/earth-engine/datasets/catalog/LANDSAT_LE07_C01_T1_SR)   or   Landsat-8

121   (https://developers.google.com/earth-engine/datasets/catalog/LANDSAT_LC08_C01_T1_SR)   images   were

122   downloaded. Within a given year the same satellite images were used. Before 1990, coverage by Landsat-5 was

123   unacceptable in this region of Afghanistan. Landsat images were directly downloaded from Google Engine

124   Archives under their *ImageCollection*. Depending on the availability of images and the year of interest, one

125   satellite or another was used (Figure 1).

Figure 1. Landsat archives used for avalanches detection since 1990.

2.3 Shuttle Radar Topography Mission-30 for Terrain Selection

Avalanche detection requires terrain parameters that were defined by using the Shuttle Radar Topography Mission-30 (https://dwtkns.com/srtm30m/). This Digital Elevation Model was collected in 2000 and is globally available on the United States Geological Survey data portal at a spatial resolution of 30 m. SRTM-30 is used in this study to delineate the regions of interest by deriving stream channels from the DEM.

2.4 Terra MODIS MOD10A2.006 for Snow Line Analysis

The ROI (regions of interest) are delineated using Terra MODIS MOD10A2.006 (https://nsidc.org/data/MOD10A2/versions/6) This product of MODIS shows the snow cover (baseline: 8 days) and is also globally available at a resolution of 500 m. MOD10A2.006 snow cover data are available since 2000. MODIS is used to extract the seasonal snow line elevations (average) during the past 20 years in the Amu Panj basin.

Terra MODIS MOD11C3.006 for Land Surface Temperature Analysis: The evolution of land surface temperature was completed using MOD11C3.006 monthly products, 0.05 degrees (https://lpdaac.usgs.gov/products/mod11c3v006/) Temperature trends were analysed from 2000 through 2021 (significance > 0.05 p-value) and the slopes were extracted and plotted on monthly maps.

2.5 Concept of the SAFE algorithm

As the aim of this study is to detect and map the annual occurrence of avalanches during the past 32 years within the study area, the monitoring approach must be reasonable and transferable from year to year. Based on frequent field observations and literature (Eckerstorfer et al., 2016) , the authors noticed that avalanches can be detected using the contrast between snow cover and bare cover, but the timing is perhaps the most important consideration.
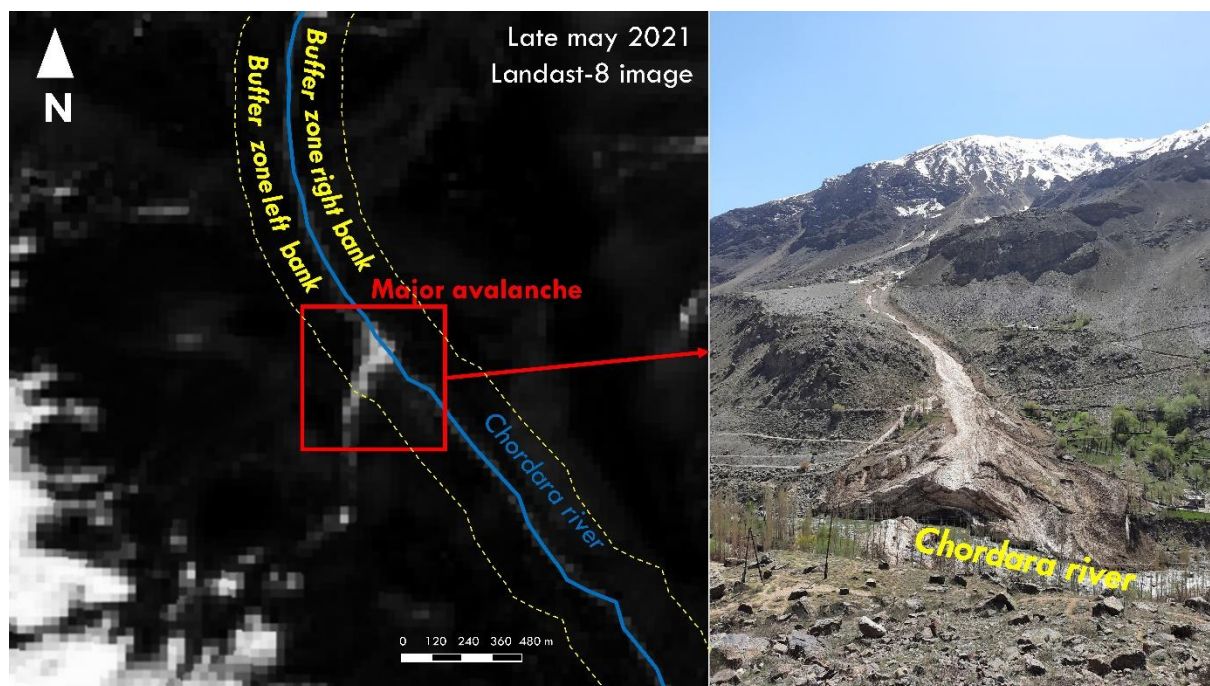
152   Indeed, the script is based on the assumption that snow packages exist in lowlands, especially along rivers and

153   streams, as late as May through mid-July. At this time of the year, the terrestrial snow cover has largely melted

154   and only snow packages triggered by avalanches remain. The location of those snow packages is also very critical

155   (i.e., along riverbanks). The avalanches are indeed detectable by delineating their depositional zones (not their

156   release or transition zones); in most cases these were located on river or stream banks as observed in the field

157   because the hillslopes always route snow avalanches in this direction. We cannot differentiate between dry, wet,

158   or powder snow because the process detects the remaining snow packages as avalanches in the late season (spring

159   and summer), not in winter, nor can we delineate multiple avalanches in the same depositional feature, only the

160   combined avalanches. In winter, we were not able to differentiate contrasts between snow cover and avalanches,

161   thus our focus on the late season.

162   *2.6 Google Engine Interface and Code Availability*

163   The concept of detecting the 'remaining snow packages in the late season' was written in Java Script using the

164   *Google Engine* platform. The script SAFE is available at:

165   https://code.earthengine.google.com/?scriptPath=users%2Farnaudcaiserman%2Fexport%3ASAFE. We selected

166   *Google Engine* for its relatively simplicity of use and open access code, which can be used by all stakeholders

167   involved in hazard and vulnerability assessments. Additionally, internet connections in remote areas, such as

168   within the Amu Panj basin, are limited and powerful computers required to run scripts and process big data are

169   sparse. Our script can be run by anyone in a reasonable amount of time, even with a low internet capacity. As an

170   example, yearly avalanches in our study area were downloaded and mapped from Badakhshan (SAFE was

171   processed from Khorog, University of Central Asia campus, in Tajikistan) in 11.3 h (about 20 min per year of

172   record) with an average connection of 2.2 Gb/s.

173

174   *2.7 Region of Interest*

175   The first step of SAFE is to define a region of interest as a mask to clip the Landsat images using SRTM-30 and

176   MOD10A2.006. Avalanche depositional deposits that terminated on riverbanks, rivers, and streams are derived

177   from SRTM-30 DEMs using *ArcHydroTool* in ArcGIS *Pro Software*. Buffers of 200 m on both sides of rivers and

178   streams are defined to: (1) catch the depositional zone of avalanches that terminate in rivers and (2) increase the

179   probability of excluding the snow coverage in higher elevations that may remain throughout the summer. As an

180   illustration, a major avalanche occurred in the border zone of Afghanistan and Tajikistan in winter 2021. The

181   remaining depositional zone was still distinct in late May and June of that year on the bank of Chordara River

182   (Figure 2).

The Cryosphere
Discussions

183

Figure 2. An illustration of avalanche detection using late snow season Landsat-8 image near Khorog in
May 2021 (Badakhshan in Tajikistan)

184
185

186   *2.8 Date Range of Interest*

187   The 200 m riparian buffer was used as a mask to clip the Landsat images. Because our area of coverage
188   encompasses very different elevations, the date of snow melt is not uniform throughout the basin. Therefore,
189   distinguishing between the depositional zone and bare land requires different times depending on elevation. To
190   accomplish this, we calculated the average elevation of the snowline for the last 20 years using MODIS products.
191   To distinguish the different melt timing between highlands from lower areas, we selected the summer snowline
192   (June-July-August; JJA). The average elevation of the JJA snowline was 4420 m during the past 20 years. Two
193   masks were therefore produced: one with a river buffer in lowlands and another for highlands. Those masks are
194   only relevant if the user carefully selects the date of interest. For lowlands (below 4420 m), our time window was
195   15 May to 15 June, indicating that the script downloads and compiles all available Landsat images acquired in this
196   range and detects avalanches efficiently because during that period the terrestrial snow cover has already melted
197   and the depositional zones are easily recognised. For higher elevations (above 4420 m), snow cover melted later;
198   dates to accurately distinguish the remaining snow packages ranged from 15 June to 15 July. After many tests, it
199   was confirmed that these date ranges reproduced the desired snow conditions during the entire 32-y period. In the
200   script, users can modify these dates (line 23 and 114) to conform to local conditions.

201

The Cryosphere
Discussions

202   *2.9 Snow Index Reclassification*

203   After the construction of the mask, SAFE proceeds as outlined in Figure 3. NDSI is selected to detect snow

204   avalanches in the script for its transferability from one Landsat generation to another. NDSI computes a ratio

205   between VIS and SWIR bands of Landsat satellites with negative NDSI representing non-snow cover and positive

206   values indicating snow coverage (Equation 1). Three cover types were distinguished to detect avalanches at the

207   correct time: (1) bare lands; (2) water bodies; and (3) snow. The values in Table 1 were established after multiple

208   tests before obtaining sufficient precision to distinguish avalanches from other land covers. On each mosaic

209   (composite of the available images during the period of interest), a cloud mask is applied using Landsat QA bands

210   in the script to remove clouds from the scene.

211   $$\frac{Band\ 4 - Band\ 6}{Band\ 4 + Band\ 6}$$ **Equation 1**

212

213   **Table 1. NDSI discrete values for avalanche detection**

Coverage	NDSI values
Bare soil	*-1 to -0.05*
Water bodies	*-0.051 to 0.30*
Snow cover	*0.31 to 1*

214

215   *2.10 Depositional Zone Selection*

216   This further step reclassifies annual NDSI layers using ranges of values in Table 1. Only 'snow cover' that

217   designates snow avalanches is selected in the script. From the selected reclassification, the script removes the

218   standalone pixels because their classification might not be precise or representative of actual cover. Next, the

219   selected 'avalanche pixels' are verified into the script avoiding manual vectorization after the downloading

220   process. The vectorization procedure of avalanches is justified by the analysis steps and post-processing after

221   downloading data. Avalanche statistics, elevations, and size are extracted from vector files. Finally, annual

222   avalanche shapefiles are exported into the Google Drive user's account.

223

Figure 3. Flow chart for Snow Avalanche Frequency Estimation (SAFE) using Landsat archives in Google

Engine.

226

2.11 Snow Avalanche Size Classification

Once the data are downloaded and imported into the GIS environment, statistical analysis commences. Every year, the number and areas of avalanches are calculated to quantify the evolution of avalanches. Moreover, the size of the avalanches is classified. Although a generic size classification exists (Greene et al., 2016), we decided to classify avalanches by size based on local conditions. We segregated four discrete categories of avalanches: small (< 1000 m²); medium (1000-5000 m^2), large (5000-15,000 m^2), and very large (15,000-100,000 m^2). Such a classification enabled us to assess the intensity of those hazards in specific locations. SAFE is not able to detect the avalanches at their time occurrence, and since these hazards are detected weeks after their occurrence, their size is underestimated by SAFE due to melting. However, the estimated sizes in SAFE are still useful for classifying avalanches by size since large snow deposits melt slower than small snow deposits. The small avalanches that occurred in winter will appear as small hazards at the time of detection and the large events as large hazards since visible snow deposits can be seen on late spring.

2.12 Validation

The performance of SAFE in correctly detecting snow avalanche depositional zones required careful assessment. To achieve this, we collected datasets that show actual locations (Global Positioning System) of avalanches that occurred in the Amu Panj basin during the last 32 years. A total of 158 snow avalanche depositional zones were

244 easily identified in the riparian buffer zones on Google Earth images in 2001, 2003, 2015, 2017, and 2019. Here

245 we used statistical measures to assess the performance of SAFE through the Probability of Detection (POD;

246 Equation 2, based on (Hafner et al., 2021)):

247

248 POD = true positive avalanches / (true positive avalanches + false negative avalanches)   **Equation 2**

249

250 where *true positive avalanches are the avalanches* detected by SAFE that were actually visible on Google Earth

251 images (in valleys were GE images were available) and *false negative avalanches* are the locations where SAFE

252 did not detect avalanches that had actually happened. Moreover, Positive Predictive Value (PPV; Equation 3) was

253 calculated to assess the number of times SAFE found an actual avalanche on the ground as follows:

254

255 PPV = true positive avalanches / (true positive avalanches + false positive avalanches)   **Equation 3**

256

257 where *false positive avalanches* are the avalanches detected by SAFE that had never happened on the ground.

258

259 The results suggest a good reliability of SAFE (Table 2). The overall POD is 0.77 which means that SAFE

260 identified a significant number of the avalanches that impacted valley bottoms. Moreover, it seems that SAFE

261 performs better in detecting true positive avalanches, avalanches that occurred on the ground, as shown by the

262 high PPV scores (average: 0.96). SAFE almost never detected snow avalanches that did not exist. However, SAFE

263 might miss some snow avalanches due to cloud cover on the Landsat images, especially in 2001 (Table 2; POD =

264 0.42 in 2001).

265

266 **Table 2. Probability of detection and Positive Predictive Values of SAFE**

Statistics	2001	2003	2015	2017	2019	Average
True positive	10	35	12	19	48	
False negative	14	6	1	4	9	
False positive	1	0	0	1	3	
POD	0.42	0.85	0.92	0.83	0.84	**0.77**
PPV	0.91	1.00	1.00	0.95	0.94	**0.96**

267

268 Another source of error arises when SAFE cannot detect avalanches due to a dark color on the snow surface

269 associated with surface debris or a debris flow on top of the avalanche. NDSI may have identified those debris

270 layers as bare soil in the classification. Based on our findings, SAFE can be considered as a conservative, yet

271   robust and efficient tool to automatically identify snow avalanche depositional zones in very remote areas and can

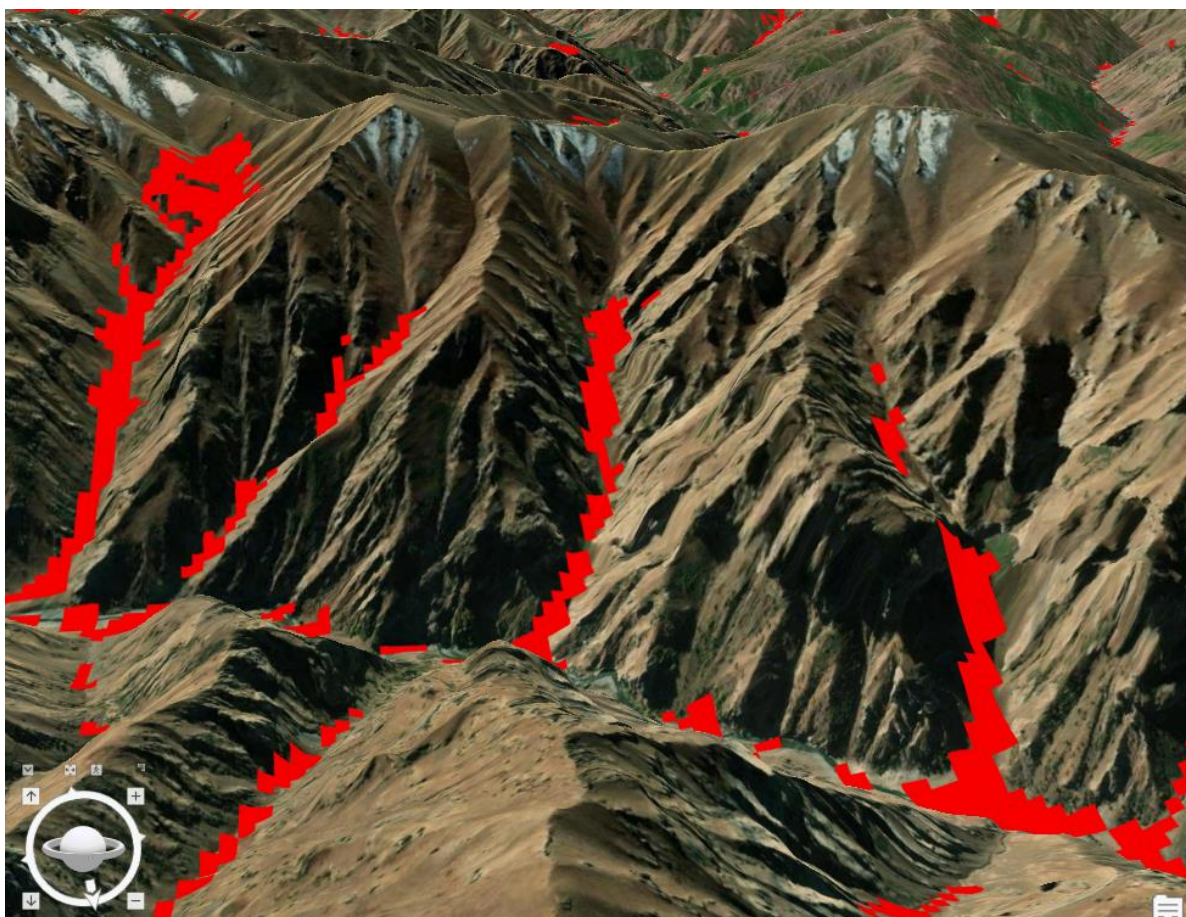272   be applied in any mountainous region.

273

274   **3. Results**

275   *3.1 Snow avalanche frequency from 1990 to 2021*

276   By compiling 32 years of satellite images (see Methodology), the frequency of avalanches at a 900 m² pixel scale

277   was determined (Figure 4 and 5a). SAFE inventories snow avalanches that occurred within a year and therefore

278   identifies the most vulnerable areas, but it does not aim to forecast future avalanches. During this period, some

279   810,000 snow avalanches impacted valleys within the Amu Panj basin (28,500 km²), i.e., approximately 28

280   avalanches km^{-2}. Each year these avalanches deposits cover an average of 1.23% of the basin area but sizes vary.

281   Avalanche size ranged from 700 to 100,000 m^2 and was categorized into four classes: small (< 1000 m²); medium

282   (1000-5000 m^2), large (5000-15,000 m^2), and very large (15,000-100,000 m^2). The most frequent are medium-size

283   avalanches; 342,000 events during the past 32 years. Our approach also identifies very large snow avalanches that

284   pose the greatest danger to local populations and infrastructure. We found no correlation between altitude of

285   depositional zones and avalanche size. Avalanches deposits in this region have an average altitude of 3820 m and

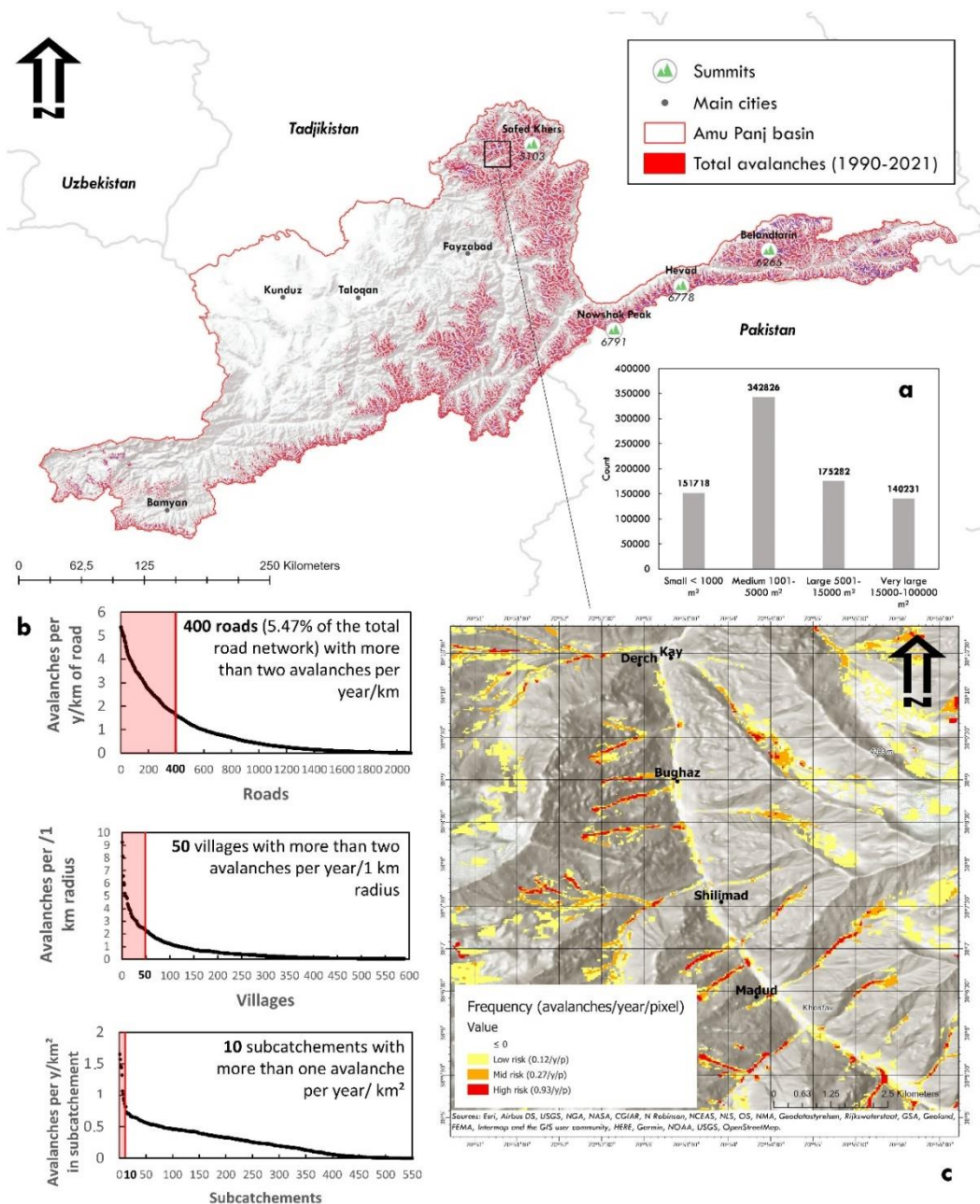286   the lowest avalanche occurred at 1755 m.

287   These spatial and temporal statistics allow for a geographic assessment of the avalanches. In total, ten sub-

288   catchments (ranging from 18 to 240 km^2) were impacted by more than one avalanche km^{-2}y^{-1}, with an average

289   frequency of 0.26 avalanches km^{-2}y^{-1} throughout the Panj Amu basin (Figure 6). More importantly, these maps

290   prioritize villages prone to avalanches and inform relevant stakeholders which villages and infrastructure are most

291   at risk. Of the 4154 villages in the region, 50 are impacted by at least one within a 1 km radius each year (Figure

292   7). These susceptible villages are in Upper Badakhshan in the north of our study area and in the Wakhan Corridor

293   in the east where the highest mountains and most remote villages are located. During the 32-y period, 92 villages

294   were affected by very large avalanches in Badakhshan and Wakhan. Since 2019, Aga Khan Agency for Habitat

295   (AKAH) is monitoring villages of Afghanistan that have been impacted by snow avalanches. In total, 217 villages

296   have been impacted by avalanches and those are located in the same vulnerable valleys detected by SAFE, namely

297   High Badakhashan and the Wakhan corridor.

298   Our remote sensing approach facilitates innovation in snow avalanche monitoring: i.e., detecting avalanches

299   outside of populated areas, especially along roads that are frequently blocked by avalanches (Figure 8). More than

300   2000 roads in the basin (5.47% of the road network) were affected by avalanches every year. Additionally, more

301   than 400 roads in Upper Badakhshan and Wakhan regions experienced more than 2 avalanches y^{-1} km^{-1} of road

302   (within a 1 km buffer). The average frequency along roads is 0.86 avalanches km^{-1}y^{-1} during the past 32 years,

303   most of these in the medium-size category.

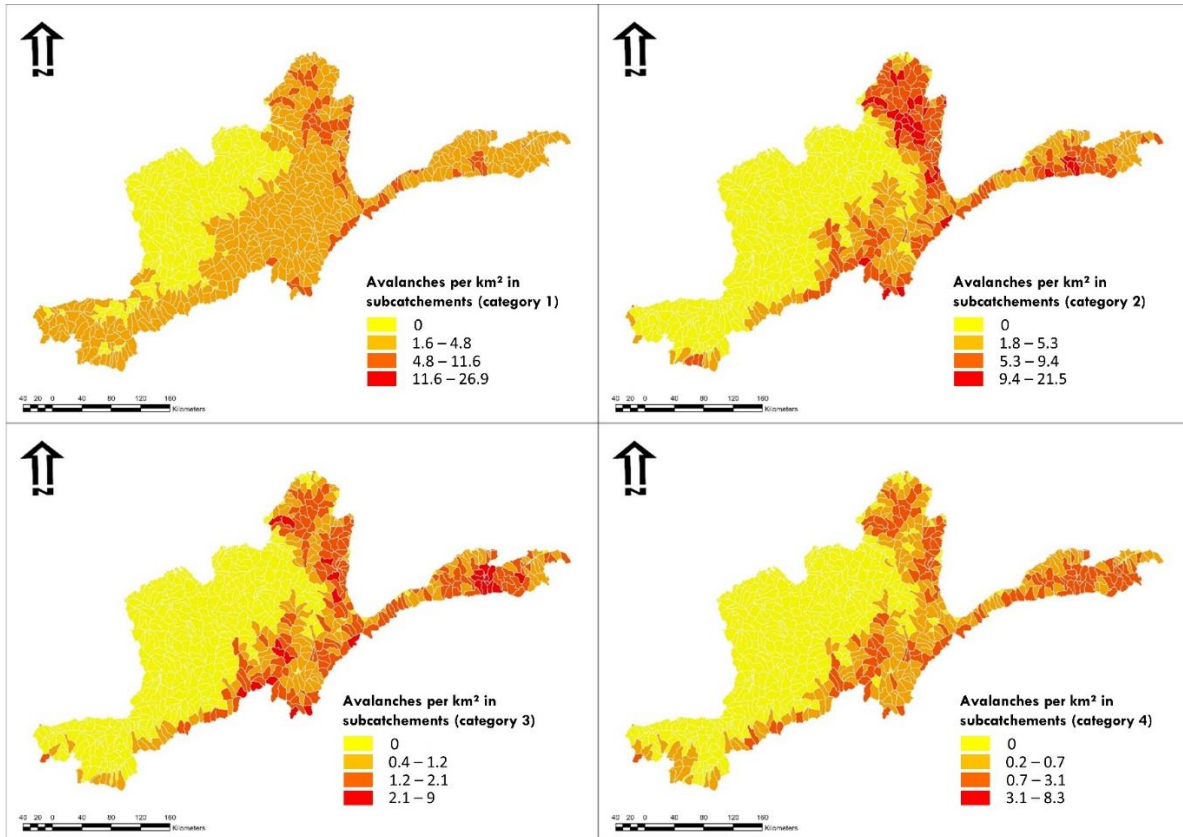**Figure 4. 3-Dimension view of the 32 years avalanches maps in Khinj village in Afghanistan (*ArcGisPro*)**

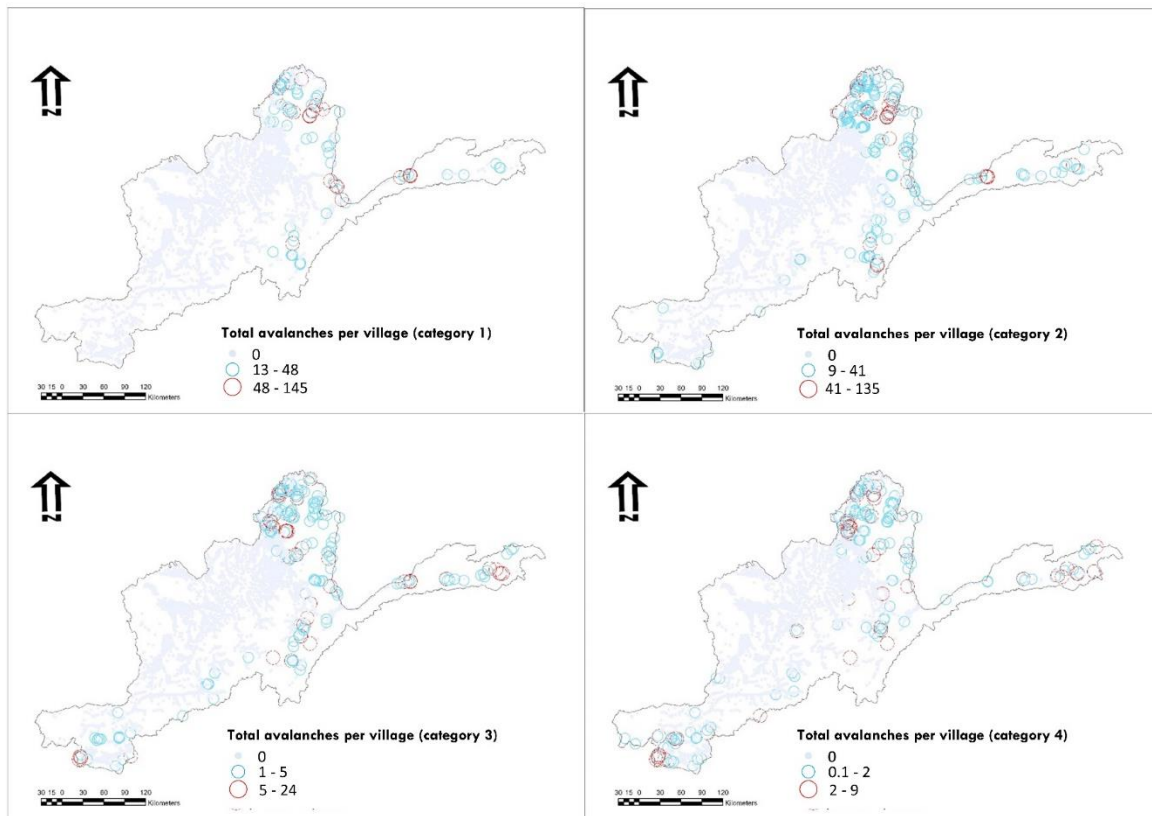**Figure 5. Yearly inventory map of snow avalanches in the Amu Panj basin: 1990-2021. a, Size classification of avalanche frequency. b, Avalanche frequency per number of roads, villages, and sub-catchments in the basin. c, An example map of avalanche frequency during the 32-y period at a village scale.**

312

313   **Figure 6. Total avalanches per category and per square kilometer in subcatchments during the past 32**

314   **years.**

14

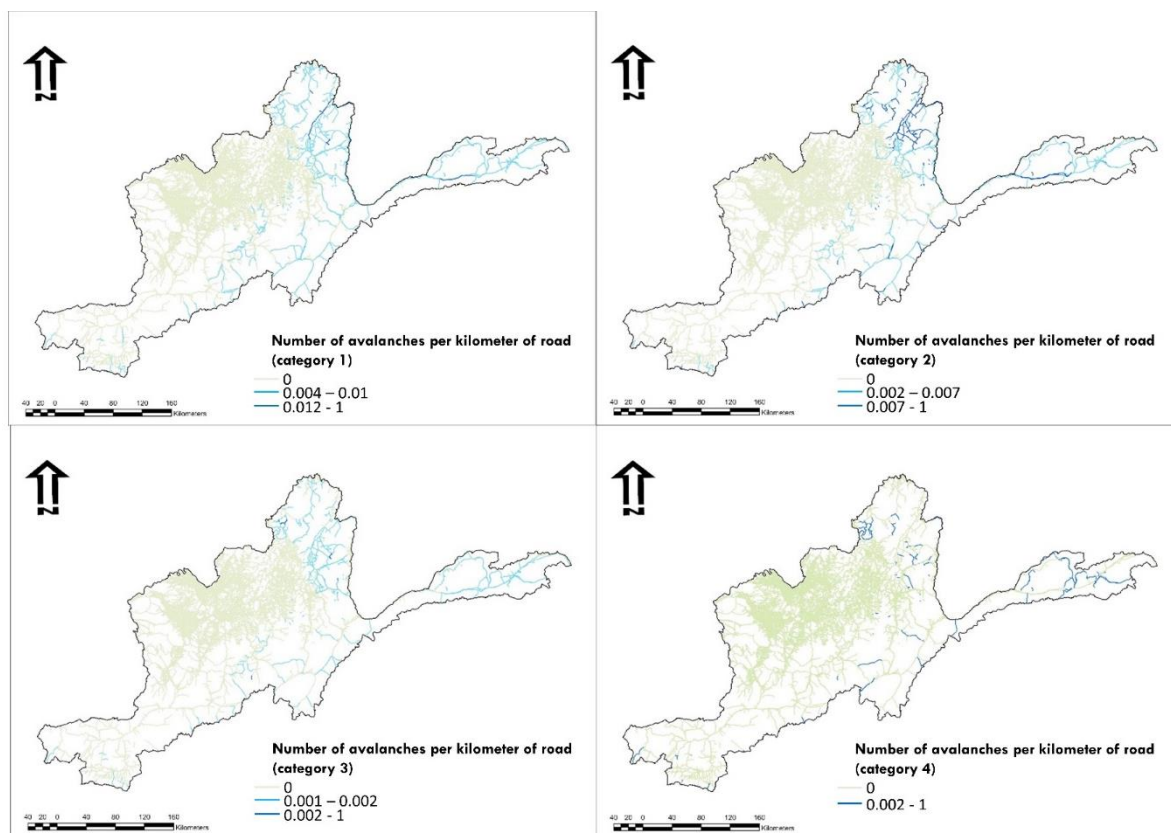**Figure 7. Total avalanches per category and per village during the past 32 years.**

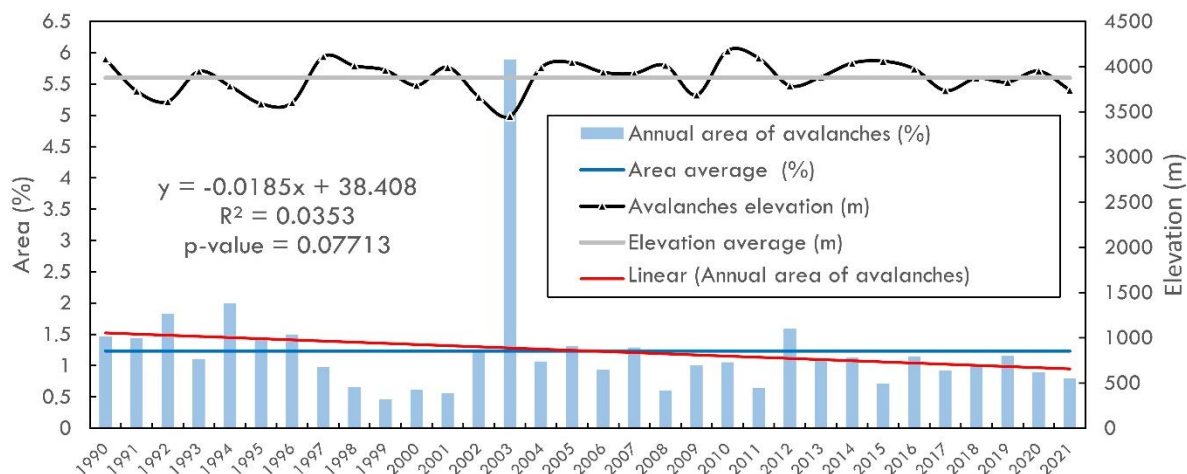**Figure 8. Total avalanches per category and per kilometer of roads during the past 32 years**

3.2 Stream blocking and resultant flooding

Damages to infrastructure and blocking of roads by avalanche depositional are not the only consequences of these mountain hazards. Because depositional zones typically reach rivers in this steep terrain, the sudden and rapid arrival of several tons of snow can temporarily block rivers inducing short-term localized flooding. By cross-checking the map of the rivers in the Amu Panj basin with SAFE outputs, it appears that 26.2% of the river network is impacted by avalanche depositional, mainly in the high mountains. During the past 32 y, 12% of the streams have been blocked by at least 10 avalanches km^{-1} representing a significant risk for villages in floodplains. The accumulated snow mass impounds river water until it can break through releasing a large discharge surge. Thus, depending on the size of the avalanche with respect to the channel dimensions, damages to villages and farmlands may occur both upstream due to impounded water (hours to weeks) and to downstream following the sudden release of water.

3.3 Snow avalanche trends during the past 32 years

This long-term monitoring of snow avalanches facilitates the assessment of the evolution of these rapid mass movements. During the 32 years of avalanche assessment, no significant temporal trends in impacted areas were detected (Figure 9). In addition, there was no significant trend of snow avalanche sizes (p-value > 0.05). Nevertheless, some years posed much greater risk than others. In the last 32 years, ten years have been more at risk with above-average avalanche coverage: 1990, 1991, 1992, 1993, 1994, 1995, 1996, 2003, 2005, 2007 and 2012. In particular, 2003 had many avalanches that occupied almost 6% of the surface area of the entire basin. That year was locally noted as having heavy snowfall and farmers benefited from more snowmelt in the spring, leading to higher than average crop yields in 2003 (FAO, 2003; Guimbert, 2004). Notably, the higher risk years were also characterised by lower altitudes for avalanches. There is a slight negative correlation (-0.55, Pearson test) between altitude and total annual avalanche area. With larger avalanche areas, depositional reaches closer to villages. For example, in 2003, the lowest avalanche occurred at an altitude of only 1871 m, very close to housing clusters and roads. It is therefore possible that communities below 2000 m are also impacted by snow avalanches and in many mountain regions of the world this represents a significant proportion of the communities living around these altitudes.

Figure 9. Snow avalanche area and elevation trend since 1990 in the Amu Panj basin. Elevation was calculated within each polygon of avalanches using SRTM-30 Digital Elevation Model. Mann-Kendall p-value 0.05 test was run to assess the significance of the trend.

3.4 Temporal geographic shifts of snow avalanches

Long-term monitoring also shows the evolution of the spatial distribution of snow avalanches. The pattern of snow avalanches has changed with time and slightly shifted to the northeast portion of the basin; thus, more avalanches are now occurring in the northeast than in the southwest (Figure 10). Nevertheless, snow coverage did not shift simultaneously according to our remote sensing analysis nor did the snowline evolve and remained variable over the last 32 years. The geographic shift of avalanches is therefore likely due snow depth evolution. Deeper snowpacks trigger snow avalanches. There are no available data on snow depth at such a scale. However, remotely sensed land surface temperature changed during the last 20 years, with a warmer band through the central portion of the basin in December (p-value 0.03 with an increase of 0.88 C°y^{-1}). This central portion is mainly mountainous and this temperature pattern may have offset the avalanches to the northern mountains of the area, while the south is characterized by lower mountains. Overall, avalanche locations tend to follow the spatial distribution of snow depth (Bühler et al., 2016). This means that despite the high variability of the snow line and snow coverage, snow avalanche distribution can significantly change over time with temperature changes and local communities must be prepared for shifting hazards.
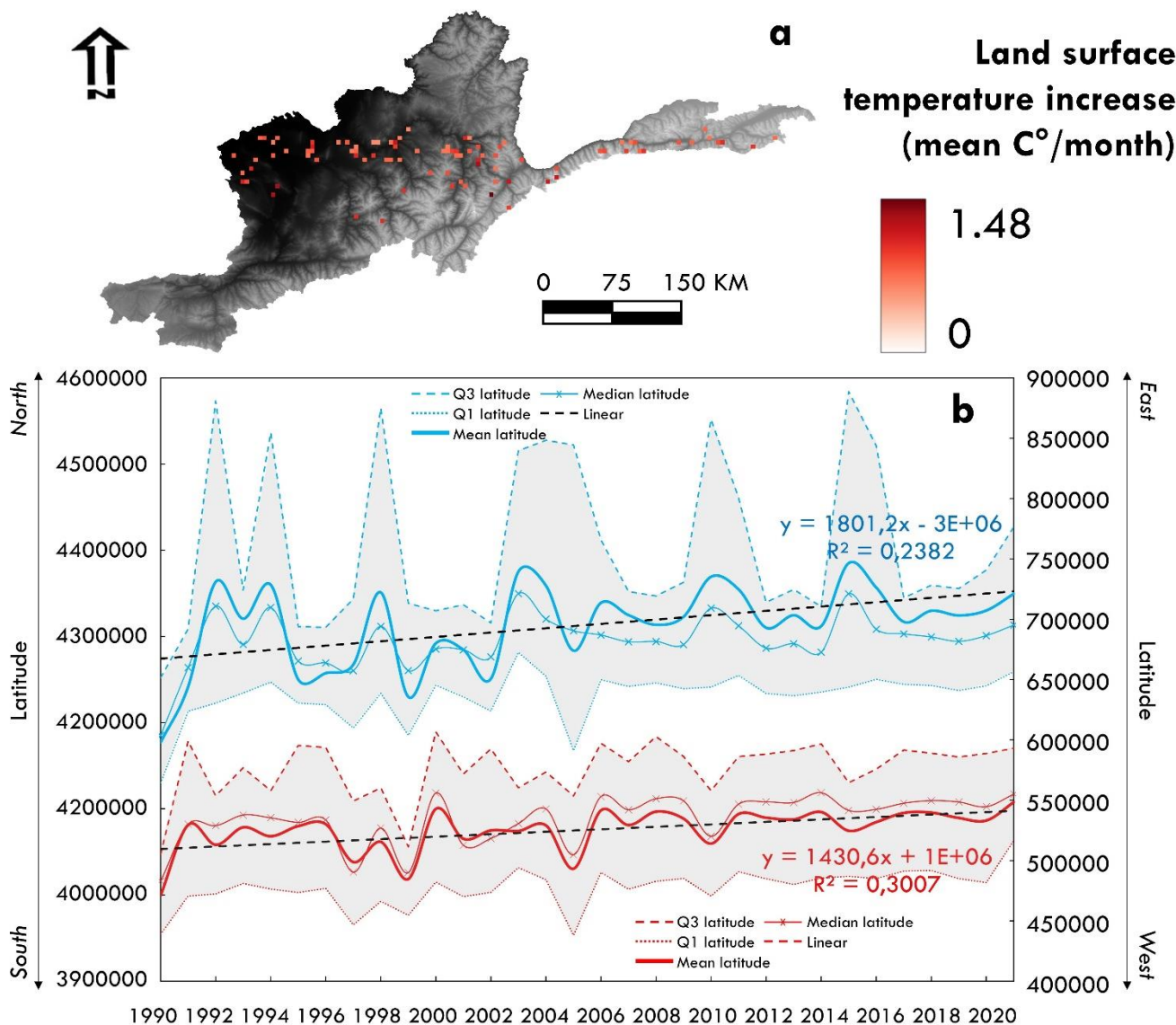
Figure 10. a, S Significant monthly temperature trend analysis in the Amu Panj Basin based on MOD11C3 products from 2000 to 2021. b, Geographical shift of avalanches: mean longitude and latitude of avalanches each year since 1990 show evidence of a movement to the northeast due to increasing temperature in winter in mountainous areas.

4. Uncertainties and implications

4.1 Sensitivity analysis of SAFE

To better understand how SAFE works and assess its performance, a sensitivity analysis was conducted between the model parameters. The number and size of avalanches vary according to the buffer used, the dates of the Landsat images, and finally

the NDSI range during the snow classification. The sensitivity analysis was conducted for the year 2019, when SAFE was most robust in valleys where actual avalanches were quite visible on Google Earth images (POD: 0.84 and PPV: 0.94). First, we run SAFE with different buffer widths (25 m of difference between each buffer). There is a strong positive correlation

380 (0.98) between the number of avalanches detected by SAFE and the buffer width (Figure 11A). The wider the buffer around the rivers, the more avalanches SAFE will find. On the other hand, the wider the buffer, the smaller the average avalanche size (positive correlation of 0.71). This is because a large buffer extends upslope where small snow patches reside, which are not avalanches since they are located at the top of hillslopes. This means that the user should not select a buffer that is too wide, rather the area should only include the riparian zone of rivers and streams where the snow avalanche deposits are located. As

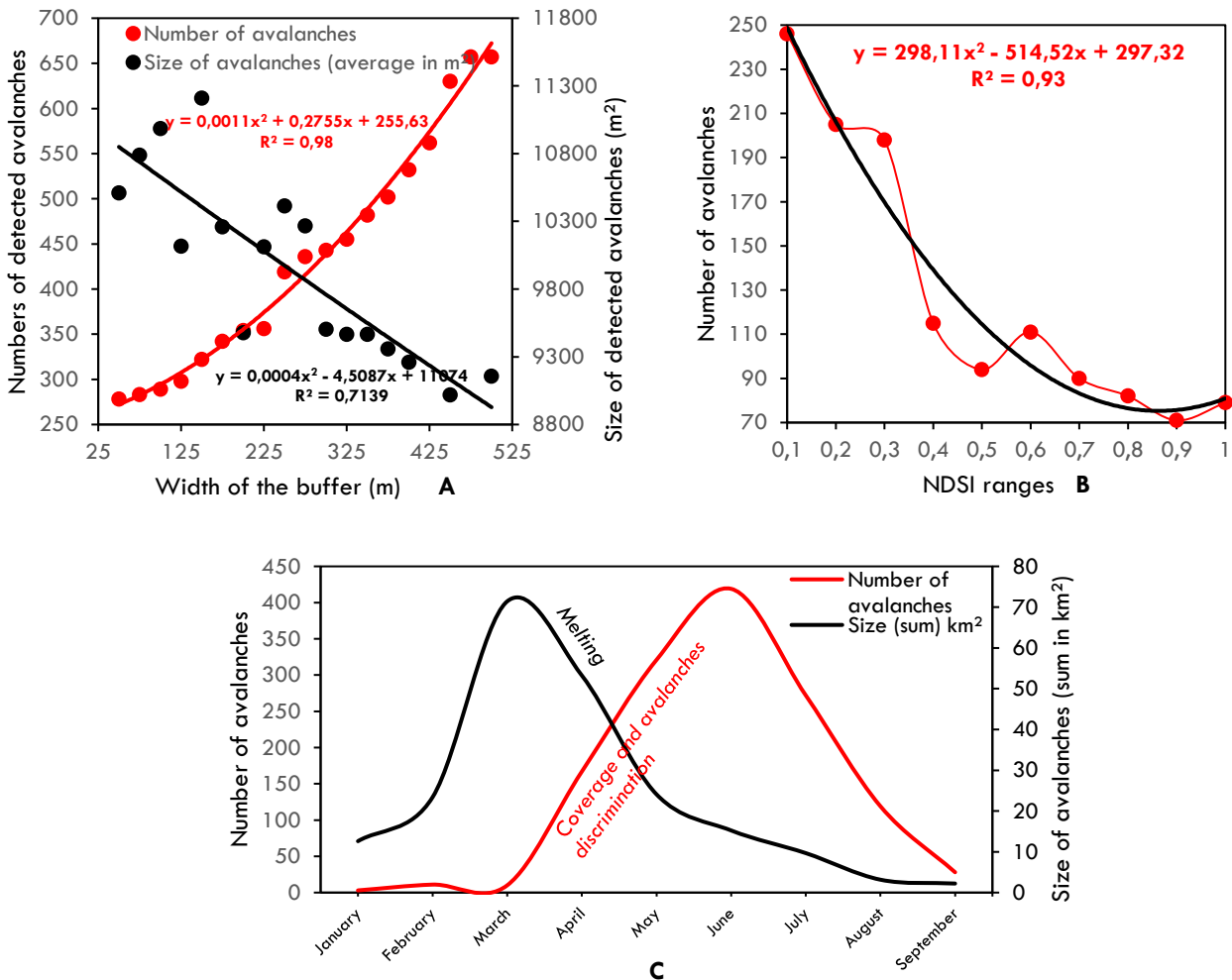385 such, we recommend a value of 200 m for the entire region studied.

Figure 11. Sensitivity tests of SAFE for number and size of detected avalanches: A, width of buffer; B, NDSI ranges;

390 **C, dates of interest**

20

The number and size of avalanches detected by SAFE depends on the NDSI range when classifying the snow. NDSI is used to differentiate between water bodies, bare lands, and snow. By varying the NDSI ranges of snow in the script, we notice a strong positive correlation with the number of avalanches detected by SAFE. The closer the index is to 0, the more hazards

395 SAFE finds. However, this correlation shows us that the choice of NDSI range is important because we notice a threshold at 0.31 (Figure 11B). Avalanches seem to be more numerous with an NDSI lower than 0.31 because the snow pixels are confused with water bodies. It is therefore essential for the user to select an NDSI higher than 0.31 to distinguish water bodies (rivers, flood areas or lakes) and snow. However, there is no correlation between the NDSI ranges and the average avalanche size as NDSI cannot interpret pixels other than 'snow' above the 0.31 threshold. Finally, the date of interest is a key parameter in

400 SAFE. In figure 11 C, we can see that the number of avalanches detected by SAFE is highest at the end of winter due to the almost constant cloud cover since January, but also due to the inability to distinguish avalanches from snow cover in winter (with Landsat images). May is a key month in SAFE applications: the snow coverage, which is thinner than the avalanche packages, begins to melt and the number of avalanches detected can then be assessed. It is therefore essential to select post-May images to detect avalanches, while taking care not to select post-July images as avalanches melt in summer and make

405 their detection impossible.

Some avalanches deposits can also be visible on successive images, after the snow coverage melted. SAFE was specifically designed to detect avalanches at their earliest stage after snow coverage melted. Indeed, starting from May (when the avalanches are not confused anymore with snow coverage), the snow deposits will start to melt and the sizes to be underestimated. For that reason, it is important to select late spring images for lowlands avalanches and early summer for high

410 lands avalanches, not later. Cloud cover is another issue in avalanches locations and sizes detection since they can partly or fully cover the avalanches at the time of the image. This is another reason to select images starting from late spring when the cloud coverage of this region is at its lowest and even null in early summer. If the cloud coverage is high even late spring, the users can still select later images, but the risk is to detect avalanches deposits that have significantly started to melt.

To summarize, we recommend the following three parameters in the SAFE script: buffer of 200 m to include only snow

415 avalanche deposits; NDSI > 0.31 to distinguish water bodies from snow, and images from May to July to distinguish avalanches from snow cover.

4.2 Excluding snow coverage

Interpreting the remaining snow packages as depositional avalanches can lead to some errors. Indeed, despite a precise masking

420 operation (excluding summits and very high plateaus where snow persists), in some cases the use of NDSI might not properly segregate avalanches from large areas of remaining snow. After assessing the sizes of true avalanches (the ones that SAFE correctly detected based on Google Earth images), it appeared that snow covers > 100,000 m² were not avalanches but snow coverage and thus we removed them. However, in highlands, even along riverbanks, some snow packages interpreted as avalanches may be remaining snow cover. As such, the date range was selected as late as possible in the year. Thus, it is

425 advised to keep the mask at the very bottom of valleys (maximum 500 m buffer along the river) to exclude high plateaus and potential snow-covered areas.

4.3 Water bodies in SAFE

A final limitation of using this remote sensing and NDSI approach for avalanche detection is the possible confusion between
430 some small water bodies and avalanches. Indeed, in some cases certain river reaches (order > 4 in our study) could be interpreted as snow because they were frozen and appeared as white pixels on the Landsat archives. The same issue can occur with ponds and lakes. This limitation was foreseen before processing the images in our study and we excluded these large water bodies from the region of interest (in the mask) by using available shapefiles. For example, Shiva Lake, one of the largest water bodies in Amu Panj basin (15 km²), was removed from the analysis. Another way to avoid the water pixel selection is
435 to adapt the NDSI reclassification itself, depending on the study area. This is possible lines 51-54 for low elevations and lines 142-144 for high elevations in the script.

4.4 SAFE outcomes compared to other snow avalanches detection studies

SAFE contributes to the literature on snow avalanche detection, but in a unique way using remote sensing. As noted, many
440 studies and models exist using various products: Radar, Optical, and Topographic. The strength of remote sensing is the automatic processing at a large scale and over long timeframes. SAFE uses the capabilities of remote sensing by processing more than one image per year at the catchment scale. Moreover, the use of Landsat archives allows assessment over the last 32 years, which is not yet possible with recent Radar data such as Sentinel-1. Most of the current avalanche detection models use freely available products, with acceptable if not good accuracy (Table 3). The accuracy of these studies using Radar images
445 ranges from 53 to 81% making this a relatively robust tool. One of the reasons why SAFE does not use Radar images is the weight of the images (data storage), especially Sentinel-1, which is mostly above 1 Gb/image. The heaviness of these images is not suitable for a model like SAFE, which was specifically designed for remote study areas where internet connections may be very limited. Other models also exist with Optical images with high accuracy ranging from 71 to 93% (Table 3). In the optical domain, SAFE showed a POD of 77% over an area of 28,500 km². SAFE is therefore in the high range of models with
450 optical, medium resolution (Landsat) images. Furthermore, one of the perspectives of this paper would be to compare the results of the different models in Table 3 with the results of SAFE over the same area where data on the size and location of avalanches would be available.

455

Table 3. References on snow avalanches accuracy using remote sensing products (Radar, Optical and Terrain)

Reference	Accuracy	Dataset
Eckerstorfer et al., 2017	75	S1
Malnes et al., 2015	53*	S1
Martinez-Vazquez	76	GB-SAR LISA
Tompkin and Leinss, 2021	81	S1
Yang et al., 2020	75**	S1
Singh et al., 2019	93	L8
Yarivan et al., 2020	90	Google Earth imagery
Hafner et al., 2021	74**	SPOT
Bühler et al., 2018	95**	DTM

460   *55 avalanches were detected using S1 image out of 102 on the field.

**POD

5. Conclusion

SAFE can be considered as a universal approach to assess snow avalanches where ground data are very limited, such as in the Afghan mountains. Here we showed the capability of long-term remote sensing data to robustly detect snow avalanches that

465   impact valley locations. While we have successively applied SAFE to assess avalanche frequency and impacts in valleys and lower hillslopes of Afghanistan, arguably one of the most data-limited regions worldwide, this model should perform even better in areas where snow data are available making it an important tool for avalanche vulnerability assessment worldwide. More than 30 years after the launch of Landsat-5, it is now possible to compile all data and assess the temporal as well as spatial evolution of such hazards. NDSI is a relevant index to detect avalanches provided the correct region and dates of interest

470   are selected - i.e., riverbanks during the late melt season. The thickness of the depositional zones facilitates the detection of avalanches after the snow cover has melted on hillslopes in spring or early summer.

The automation of snow avalanche detection using remote sensing technologies at regional scales is still new and SAFE was designed to guide decision-makers, planners, and disaster risk practitioners. Indeed, such people can now know where the most at-risk areas are located based on these frequency maps. Such information informs the relative risk of building sites and land

475   use decisions in such mountainous terrain with greater precision. The level of exposure of roads to avalanches can also be estimated using these frequency maps, and can inform road managers regarding road location, maintenance practices, and mitigation structures. The tourism sector can also benefit from this snow avalanche inventory, especially the winter sports industry. Furthermore, this method can also be used to prioritize areas for more sophisticated and data-intensive avalanche risk analysis (Keylock et al., 1999). SAFE can be applied by any user throughout mountainous regions of the world as it is designed

480   to be user-friendly. Thus, frequent users can contribute to the robustness of the snow avalanche archive, thus improving recommendations to policy makers.

The Cryosphere
Discussions

Open Access

EGU

Author contributions

485 A.C. designed the concept of SAFE method, wrote the Google Engine script and processed the analyses of snow avalanches. A.C. and R.C.S. participated the conception of SAFE and all authors helped interpret the results. D.R.G. contributed to the writing and provided the AKAH dataset of impacted villages by snow avalanches. A.C. and R.C.S. wrote the paper.

Competing interests

490 The authors declare that they have no conflict of interest.

Acknowledgements

References

Abermann, J., Eckerstorfer, M., Malnes, E., Hansen, B.U., 2019. A large wet snow avalanche cycle in West Greenland quantified using remote sensing and in situ observations. Nat Hazards 97, 517–534. https://doi.org/10.1007/s11069-019-03655-8

500 Asad Sarwar, Q., 2002. Water resources management in Afghanistan: the issues and options. International Water Management Institute, Pakistan.

Bair, E.H., Rittger, K., Ahmad, J.A., Chabot, D., 2020. Comparison of modeled snow properties in Afghanistan, Pakistan, and Tajikistan. The Cryosphere 14, 331–347. https://doi.org/10.5194/tc-14-331-2020

505 Bühler, Y., Adams, M.S., Bösch, R., Stoffel, A., 2016. Mapping snow depth in alpine terrain with unmanned aerial systems (UASs): potential and limitations. The Cryosphere 10, 1075–1088. https://doi.org/10.5194/tc-10-1075-2016

Bühler, Y., von Rickenbach, D., Stoffel, A., Margreth, S., Stoffel, L., Christen, M., 2018. Automated snow avalanche release area delineation – validation of existing algorithms and proposition of a new object-based approach for large-scale hazard indication mapping. Natural Hazards and Earth System Sciences 18, 3235–3251.
510 https://doi.org/10.5194/nhess-18-3235-2018

Chabot, D., Kaba, A., 2016. Avalanche forecasting in the Central Asian countries of Afghanistan, Pakistan and Tajikistan. Presented at the International Snow Science Workshop, Breckenridge, Colorado.

Colorado Avalanche Information Center, 2021. Avalanche.org » Accidents [WWW Document]. Avalanche.org. URL https://avalanche.org/avalanche-accidents/ (accessed 6.30.21).

515 Deems, J.S., Painter, T.H., Finnegan, D.C., 2013. Lidar measurement of snow depth: a review. Journal of Glaciology 59, 467–479. https://doi.org/10.3189/2013JoG12J154

Eckerstorfer, M., Bühler, Y., Frauenfelder, R., Malnes, E., 2016. Remote sensing of snow avalanches: Recent advances, potential, and limitations. Cold Regions Science and Technology 121, 126–140. https://doi.org/10.1016/j.coldregions.2015.11.001

520 Eckerstorfer, M., Malnes, E., Frauenfelder, R., Doomas, U., Brattlien, K., 2014. Avalanche Debris Detection Using Satellite-Borne Radar and Optical Remote Sensing. International Snow Science Workshop 2014 Proceedings, Banff, Canada 131–138.

Eckerstorfer, M., Malnes, E., Müller, K., 2017. A complete snow avalanche activity record from a Norwegian forecasting region using Sentinel-1 satellite-radar data. Cold Regions Science and Technology, International Snow Science Workshop 2016 Breckenridge 144, 39–51. https://doi.org/10.1016/j.coldregions.2017.08.004

European Avalanches Warning Services, 2021. Fatalities [WWW Document]. EAWS. URL https://www.avalanches.org/fatalities/ (accessed 6.30.21).

FAO, 2003. FAO global information and early warning system on food and agriculture - world food programme [WWW Document]. URL https://www.fao.org/3/j0156e/j0156e00.htm (accessed 10.17.21).

GFDRR, 2018. Afghanistan Multi-Hazard Risk Assessment. World Bank, Kabul, Afghanistan.

Greene, E., Birkeland, K., Elder, K., McCammon, I., Staples, M., Sharaf, D., 2016. Observation Guidelines for Avalanche Professionals in the U.S. American Avalanche Association (No. ISBN-13: 978-0-9760118-1-1). Pagosa Springs, Victor, United States of America.

Gubler, H., 1987. Measurements and modelling of snow avalanche speeds, in: Proceedings of the Davos Symposium. Presented at the Avalanche Formation, Movment and Effects, Davos.

Guimbert, S., 2004. Struture and performance of the Afghan economy. World, Washington D.C, United States.

Hafner, E.D., Techel, F., Leinss, S., Bühler, Y., 2021. Mapping avalanches with satellites – evaluation of performance and completeness. The Cryosphere 15, 983–1004. https://doi.org/10.5194/tc-15-983-2021

Hammond, J.C., Saavedra, F.A., Kampf, S.K., 2018. Global snow zone maps and trends in snow persistence 2001–2016. International Journal of Climatology 38, 4369–4383. https://doi.org/10.1002/joc.5674

Islamic Republic of Afghanistan Governmental Website, 2021. Badakhshan [WWW Document]. English. URL https://president.gov.af/en/badakhshan/ (accessed 8.31.21).

Keylock, C.J., McClung, D.M., Magnusson, M.M., 1999. Avalanche risk mapping by simulation. Journal of Glaciology 303–314.

Kravtsova, V.I., 1990. Snow Cover Mapping of Afghanistan's Mountains with Space Imagery. Mapping Sciences and Remote Sensing 27, 295–302. https://doi.org/10.1080/07493878.1990.10641815

Louge, M.Y., Turnbull, B., Carroll, C., 2012. Volume growth of a powder snow avalanche. Annals of Glaciology 53, 57–60. https://doi.org/10.3189/2012AoG61A030

Malnes, E., Eckerstorfer, M., Vickers, H., 2015. First Sentinel-1 detections of avalanche debris. The Cryosphere Discussions 9, 1943–1963. https://doi.org/10.5194/tcd-9-1943-2015

Martinez-Vazquez, A., Fortuny-Guasch, J., 2008. A GB-SAR Processor for Snow Avalanche Identification. IEEE Transactions on Geoscience and Remote Sensing 46, 3948–3956. https://doi.org/10.1109/TGRS.2008.2001387

Mohanty, A., Hussain, M., Mishra, M., Kattel, D.B., Pal, I., 2019. Exploring community resilience and early warning solution for flash floods, debris flow and landslides in conflict prone villages of Badakhshan, Afghanistan. International Journal of Disaster Risk Reduction 33, 5–15. https://doi.org/10.1016/j.ijdrr.2018.07.012

OCHA-United Nations, 2012. DistrictsAffectedbyAvalanches -Badakhshan Province19Jan.2012.

Prokop, A., 2008. Assessing the applicability of terrestrial laser scanning for spatial snow depth measurements. Cold Regions Science and Technology, Snow avalanche formation and dynamics 54, 155–163. https://doi.org/10.1016/j.coldregions.2008.07.002

Prokop, A., Schön, P., Singer, F., Pulfer, G., Naaim, M., Thibert, E., 2013. Determining Avalanche Modelling Input Parameters Using Terrestrial Laser Scanning Technology. International Snow Science Workshop Grenoble – Chamonix Mont-Blanc - October 07-11, 2013 770–774.

Schaffhauser, A., Adams, M., Fromm, R., Jörg, P., Luzi, G., Noferini, L., Sailer, R., 2008. Remote sensing based retrieval of snow cover properties. Cold Regions Science and Technology, Snow avalanche formation and dynamics 54, 164–175. https://doi.org/10.1016/j.coldregions.2008.07.007

Singh, D.K., Mishra, V.D., Gusain, H.S., Gupta, N., Singh, A.K., 2019. Geo-spatial Modeling for Automated Demarcation of Snow Avalanche Hazard Areas Using Landsat-8 Satellite Images and In Situ Data. J Indian Soc Remote Sens 47, 513–526. https://doi.org/10.1007/s12524-018-00936-w

Singh, K.K., Singh, D.K., Thakur, N.K., Dewali, S.K., Negi, H.S., Snehmani, Mishra, V.D., 2020. Detection and mapping of snow avalanche debris from Western Himalaya, India using remote sensing satellite images. Geocarto International 0, 1–19. https://doi.org/10.1080/10106049.2020.1762762

Smith, W.D., Dunning, S.A., Brough, S., Ross, N., Telling, J., 2020. GERALDINE (Google Earth Engine supRaglAciaL Debris INput dEtector): a new tool for identifying and monitoring supraglacial landslide inputs. Earth Surface Dynamics 8, 1053–1065. https://doi.org/10.5194/esurf-8-1053-2020

575 Tompkin, C., Leinss, S., 2021. Backscatter Characteristics of Snow Avalanches for Mapping With Local Resolution Weighting. IEEE Journal of Selected Topics in Applied Earth Observations and Remote Sensing 14, 4452–4464. https://doi.org/10.1109/JSTARS.2021.3074418

USAID, 2021. Afghanistan Avalanches [WWW Document]. URL http://afghanistanavalanches.org/ (accessed 6.30.21).

World Bank, 2017. Climate in Crisis: How Risk Information Can Build Resilience in Afghanistan [WWW Document]. URL
580 https://blogs.worldbank.org/endpovertyinsouthasia/climate-crisis-how-risk-information-can-build-resilience-afghanistan (accessed 6.30.21).

Yang, J., Li, C., Li, L., Ding, J., Zhang, R., Han, T., Liu, Y., 2020. Automatic Detection of Regional Snow Avalanches with Scattering and Interference of C-band SAR Data. Remote Sensing 12, 2781. https://doi.org/10.3390/rs12172781

Yariyan, P., Avand, M., Abbaspour, R.A., Karami, M., Tiefenbacher, J.P., 2020. GIS-based spatial modeling of snow
585 avalanches using four novel ensemble models. Science of The Total Environment 745, 141008. https://doi.org/10.1016/j.scitotenv.2020.141008

Zhang, J., Gurung, D.R., Liu, R., Murthy, M.S.R., Su, F., 2015. Abe Barek landslide and landslide susceptibility assessment in Badakhshan Province, Afghanistan. Landslides 12, 597–609. https://doi.org/10.1007/s10346-015-0558-5

590